Interplay between magnetic domain patterning and anisotropic magnetoresistance probed by magneto-optics

J. Osten,[1,2,*] K. Lenz,[1] H. Schultheiss,[1,2] J. Lindner,[1] J. McCord,[3] and J. Fassbender[1,2]

[1]*Helmholtz-Zentrum Dresden-Rossendorf, Institute of Ion Beam Physics and Materials Research, Bautzner Landstraße 400, 01328 Dresden, Germany*

[2]*Institute for Physics of Solids, Technische Universität Dresden, Zellescher Weg 16, 01069 Dresden, Germany*

[3]*Kiel University, Institute for Materials Science, Kaiserstraße 2, 24143 Kiel, Germany*

We study the correlation between the magnetic reversal and the anisotropic magnetoresistance (AMR) response in magnetic hybrid structures that were created by local modification of magnetic properties induced by ion implantation. The stripe pattern has been investigated simultaneously by dual-wavelength Kerr microscopy and magnetoresistance measurements. We observe that the switching of the stripe pattern introduces an additional AMR maximum. The domain wall in between the stripes provides a positive resistance contribution, whereas domains at the stripe edges lead to an asymmetric AMR response. A method for calculating the AMR response from the quantitative Kerr micrographs is demonstrated that allows the reconstruction of the AMR value within a region of interest only.

I. INTRODUCTION

Magnetoresistance effects are the base of nowadays magnetic sensors. Tailoring their properties is of highest technological relevance and can be achieved by, e.g., local modification of magnetic parameters [1,2]. This modification can influence the behavior of the magnetic domains in the material. Also other kinds of manipulation of the magnetoresistance are possible [3–5]. The orientation of the magnetization with respect to the current direction determines the magnitude of the anisotropic magnetoresistance (AMR), as already discovered by Thomson in 1857 [6]. For most of the materials the resistance is high when the magnetization is aligned with the electrical current direction as this configuration has the highest probability of s-d scattering of the electrons. The resistance is low when the magnetization is perpendicular to the current. With the AMR signal of a simple unpatterned film it is not possible to detect the polarity of a magnetic field. An antisymmetric dependence can be achieved by using a barber pole structure [7]. Another approach is the use of multilayer stacks consisting of two AMR films with different anisotropies [8]. Manipulation of the anisotropy has a direct effect on the magnetic domains. Therefore, the occurrence of magnetic domains and the resulting AMR response is highly correlated.

Magnetic stripes or hybrid structures have been investigated. They can be employed for various applications, for example in the field of magnonics to modify the spin-wave propagation [9,10], for the creation of a lateral exchange spring system [11], and to determine the exchange constant [12]. Manago *et al.* investigated the magnetoresistance of a zigzag shaped nanowire [13]. It was shown that the domain-wall resistance originates from the AMR. The contribution of the intrinsic domain wall to the resistance is under discussion. It is not clear whether the intrinsic domain walls give a negative contribution [14,15] or a positive contribution [16,17] to the resistance. Truetzschler *et al.* measured a hybrid structure consisting of an ion modified exchange coupled ferromagnet-antiferromagnet film and additionally calculated the AMR response [18]. Their finding was that it is possible to use ion implantation to create a unique angular magnetoresistance dependence. The reversal of an L-shaped permalloy nanowire was investigated by Beguivin *et al.* [19]. In other experiments [20,21] the AMR was measured to evaluate the magnetostatic interaction or to investigate domain walls in a permalloy nanowire. These investigations were performed on single wires or hybrid structures where the magnetic domain structures, for which—in contrast to our work—the domain configurations were not observed at the same time. For direct comparison of the AMR and the magnetic domain configuration we measured them simultaneously combining magnetoresistance measurements with Kerr microscopy imaging [22].

In this work, the investigated samples consist of laterally alternating stripes of pure permalloy and ion-implanted permalloy. The arrangement of stripes results in a more complex AMR result compared to a single stripe due to exchange interaction and domain walls at the stripe edges. In our experimental approach the AMR is measured *while* observing the magnetic domains by dual-wavelength Kerr microscopy. We investigate the dependence of the AMR for the hybrid structures on different parameters, like stripe width and magnetic field angle. A key question to answer was whether the domain walls provide a negative or positive contribution to the resistance and which effect is dominating the domain-wall resistance: the anisotropic magnetoresistance or the intrinsic part. Another question was if the antisymmetric AMR response can be created by a hybrid structure.
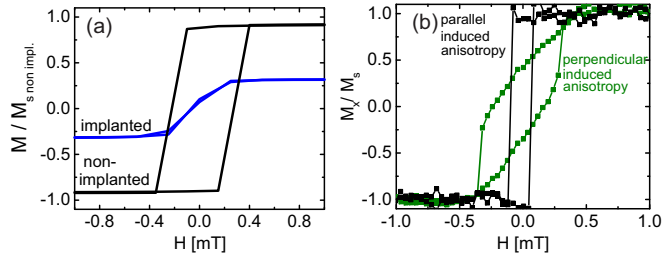
*j.osten@hzdr.de

FIG. 1. (a) VSM measurements with the field applied parallel to the induced anisotropy axis for the nonimplanted film (black curve) and implanted film (blue curve). (b) Magnetization with external field applied parallel to the induced anisotropy (black curve) and perpendicular to it (green curve).

The experimental details are explained in the following section. The measurements are shown and discussed in Sec. III and summarized in Sec. IV.

II. EXPERIMENTAL DETAILS

A. Sample preparation

The permalloy hybrid stripe samples were fabricated by dc-magnetron sputter deposition in a multisource high vacuum sputter system in IPHT Jena. At first, a 20-nm-thick $Ni_{80}Fe_{20}$ (permalloy) magnetic film was deposited onto Si(001) substrate. The Ar pressure was 5.2×10^{-3} mbar. During this step a small magnetic field was applied to introduce a uniaxial magnetic anisotropy. This induced anisotropy is a field-induced anisotropy of uniaxial character. A proof is shown in Fig. 1(b). The magneto-optical Kerr effect measurements display an easy axis loop parallel to the induced anisotropy direction of the permalloy film, while the magnetically harder loop is obtained when the field is applied perpendicular to the direction of the induced anisotropy. In the next step a stripe pattern of resist was created by means of optical lithography. The partially resist covered samples were implanted by Cr^+ ions at a fluence of 1×10^{16} Cr^+/cm^2 and a kinetic energy of 15 keV. Thus, only the uncovered parts of the permalloy film were modified by the Cr^+ ions. The implantation with Cr leads in this case to a saturation magnetization of 36% of the original value and to a reduction of the induced anisotropy [Fig. 1(a)]. From the bulk phase diagram it is known that Cr implantation results in a reduction of the Curie temperature, and hence at a fixed temperature to a reduction of the magnetic moment [23] and reduces the induced anisotropy of the permalloy film. If the Cr concentration in the permalloy reaches 8% the Curie temperature is already reduced below room temperature [24]. To achieve a single domain state within each stripe a large length-to-width ratio is important [25]. To fulfill this condition the stripe length was set to 5 mm and the width to a few micrometers. Different stripe structures with various widths were prepared (see Fig. 2), considering that a reduction of the stripe width increases the saturation field [25].

B. Measurement setup

Dual-wavelength Kerr microscopy, which is based on the magneto-optical Kerr effect, is used to observe the magnetic
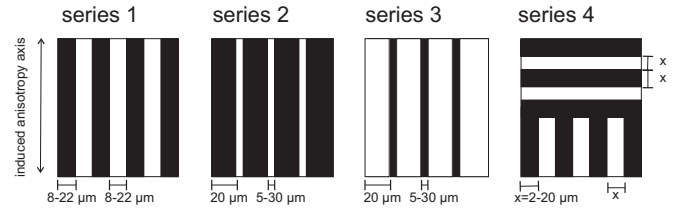

FIG. 2. Sketch of the four different sample layouts. The stripe width is given in μm. Black (white) color represents implanted (nonimplanted) stripes. The double headed arrow denotes the induced anisotropy axis.

domains and to record the magnetic reversal curve of the sample section in the field of view around 0.03 mm^2 quantitatively. By aligning one fiber output at the x position of the aperture plane and the second fiber output at the y position of the aperture plane it is possible to measure the longitudinal magneto-optical Kerr effect with s-polarized and p-polarized light at the same time. Detailed information about the magneto-optical Kerr effect and dual-wavelength Kerr microscopy can be found in this review (Secs. 3.2.2 and 5 of Ref. [26]). The setup consists of a Zeiss polarization microscope equipped with a quadrupole electromagnet. The sample holder is equipped with electrical contacts in two-point geometry and final contact to sample is realized with conducting paste and copper tape. The resistance was measured by a source meter unit consisting of a current source and a nanovoltmeter. The quantitative Kerr imaging combined with simultaneous resistance measurements allows for a detailed investigation of the interplay of magnetic domains and the AMR [22].

III. RESULTS AND DISCUSSION

A. Influence of the stripe structure on the AMR

In Fig. 3 the AMR and the simultaneously measured magnetization reversal images are displayed for one sample with the implanted stripe width of 20 μm and the nonimplanted of 15 μm [27]. The measured resistance was normalized to the resistance R_s of the sample measured at magnetic saturation in the chosen field direction. The current was applied perpendicular to the long edge of the stripes in all experiments (as indicated by the red dotted arrows). This direction was chosen to make the current pass all interfaces between the implanted and nonimplanted stripes, due to which the influences of domain walls (in series) on the AMR become more relevant than for the case of a parallel current flow.

The red dotted lines mark the field values for which the Kerr micrography images are presented in the lower panels. The small alternating black (white) rectangles below the domain images mark the regions of implanted (nonimplanted) stripes. The green curve (M_x) is the magnetization component perpendicular to the long axis of the stripe. Here the AMR (orange curve) is reduced during the magnetization reversal. The same value is obtained for positive and negative saturation field values. The magnetization reversal (green curve) of the x component reveals a magnetization rotation with a small jump. If the x component of the magnetization along the current
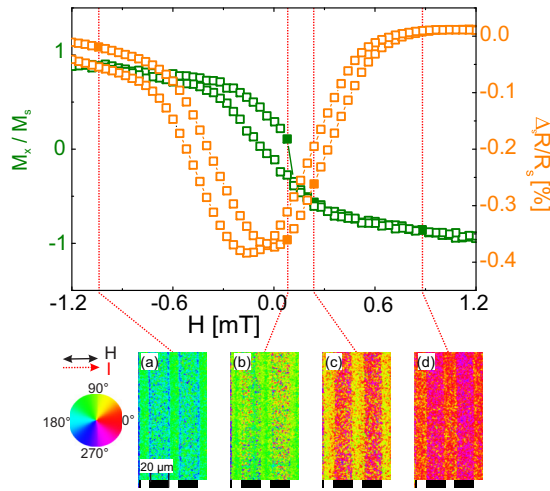
FIG. 3. x component of M perpendicular to the main stripe axes (green squares) and relative resistance change (orange squares) as a function of applied field sample with $w = 20\,\mu\mathrm{m}\,|\,15\,\mu\mathrm{m}$ (implanted | nonimplanted) stripes at $\varphi_H = 0°$. The field (current) direction is denoted by a black (dashed red) arrow. (a)–(c) Corresponding domain images taken at field values marked with dotted lines in the upper panel. The color code denotes the magnetization direction. Black (white) rectangles mark implanted (nonimplanted) stripes. Note that only one field sweep direction (from negative to positive field) value is shown for the images.
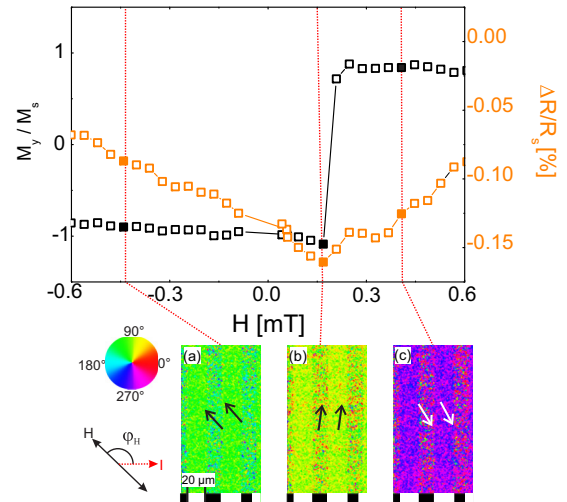

FIG. 4. y component of M (along stripe length) (black squares) and relative resistance change (orange squares) as a function of applied field for a sample with $w = 15\,\mu\mathrm{m}\,|\,20\,\mu\mathrm{m}$ (implanted | nonimplanted) stripes at $\varphi_H = 135°$. R_s is the resistance of the sample measured at magnetic saturation in $\varphi_H = 135°$ direction. The field (current) direction is denoted by black (dashed red) arrows. (a)–(c) Corresponding domain images taken at field values marked with dotted lines in the upper panel. The color code denotes the magnetization direction. Black (white) rectangles mark implanted (nonimplanted) stripes. Only one field sweep direction (from negative to positive field) value is shown for the images.

direction is large (small), the resistance becomes large (small). Moreover, the rotation of the magnetization corresponds to the observed AMR behavior. The domain configurations shown in Figs. 3(a)–3(d) show that the magnetization is first oriented closer towards the current direction and subsequently aligns with the stripe axis [Fig. 3(b)] and in the end back again in the current direction [Fig. 3(c)]. The ion implantation results also in a reduction of the Kerr signal, explaining the somewhat smaller signal-to-noise ratio within the Kerr images of the implanted stripes. It, moreover, becomes evident that the magnetization process of the narrow stripes differs slightly from the wider implanted stripes [best seen in Fig. 3(c)]. This is a result of the larger shape anisotropy of the narrower stripes, leading to larger saturation fields. For a better visibility only the field sweep from negative to positive field values is displayed in the following measurements.

In order to achieve a larger AMR effect from different domain patterns, in the next step the field was applied at an angle of $\varphi_H = 135°$. In the upper panel of Fig. 4 a steplike easy axis magnetization reversal is observed in the M_y component parallel to the long stripe axes. During the magnetization reversal the resistance is decreased (Fig. 4, lower panel). At negative field values the magnetization is oriented along the field direction at $\varphi_H = 135°$ [Fig. 4(b)]. Hence, the resistance is high. Then the magnetization turns into the stripe direction parallel to the shape anisotropy [Fig. 4(b)] leading to a decrease of the resistance. After the switching, the magnetization is again oriented in the field direction [Fig. 4(c)], resulting in an increase of the AMR. This example prooves that the two different kinds of stripes reorient collectively.

Next we investigate the situation for 20-μm-wide implanted, 15-μm-wide nonimplanted stripes. Again, the field angle was

set to $\varphi_H = 135°$ and only one direction of field sweep is displayed. The magnetization component along the stripe axes (y component) is monitored (black curve in Fig. 5, upper panel), exhibiting a two-step switching process. At the first step the magnetization in one part of the sample switches while the remaining regions within the sample switch in a second step at higher fields. Such a two-step switching process has been reported before for a smaller stripe width at a different field angle [28]. As a consequence, it is possible to manipulate the magnetization behavior drastically by using a different stripe width.

The AMR (orange curve in Fig. 5) is decreasing during the magnetization reversal but exhibits an additional local maximum. The comparison of the magneto-optical Kerr effect and resistance measurements reveals that the maximum occurs during the first step of the two-step switching process. The origin of the additional peak and the two-step switching can be understood by taking the domain images into account.

In saturation the resistance reaches the same value as measured for negative saturation field (not shown). The magnetization inside both stripes is oriented parallel to the stripe edges, resulting in a resistance minimum [Fig. 5(a)]. The resistance is highest when the magnetization aligns within the current direction. Hence, a rotation of the magnetization component into the current direction leads to an increase of the resistance. Indeed, in Fig. 5(b) the magnetization starts to rotate into current direction, resulting in an increase of the resistance. As a result of the reduced saturation magnetization of the implanted stripes they switch before the nonimplanted ones [Fig. 5(c)] [29]. This separate switching of different stripe types manifests itself in the two-step shape of the hysteresis loop (black curve in Fig. 5, upper panel). Also the maximum
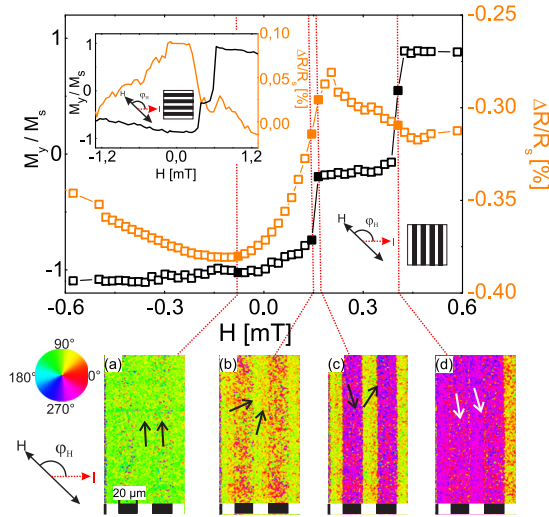
FIG. 5. y component of M (along stripe length) (black squares) and relative resistance change (orange squares) as a function of the applied field for sample with $w = 20$ μm | 15 μm (implanted | nonimplanted) stripes at $\varphi_H = 135°$. The field (current) direction is denoted by a black (dashed red) arrow. (a)–(d) Corresponding domain images taken at field values marked by dotted lines in the upper panel. Black (white) rectangles mark implanted (nonimplanted) stripes. Only one field sweep direction from negative to positive field values is shown. The inset shows the measurements of the M component the along stripe length (black line) and relative resistance change (orange line) when the current is applied parallel to the stripe axis. R_s is the resistance of the sample measured at saturation for the chosen field direction.

of the resistance is directly connected to a separate switching process. When the resistance shows the additional maximum a Néel-type domain wall [30] is present between the implanted and the nonimplanted stripes. The presence of Néel-domain walls, compared to the Bloch type, is favored because of the magnetization being confined within the film plane due to the small film thickness. For a material with higher cubic anisotropy, like epitaxial Fe, it was possible to determine the intrinsic domain-wall resistance [31]. But in a low anisotropy material, like permalloy, the Néel-domain walls have extended tails. This means that the transition between the magnetic domain and the domain-wall core is rather smooth, which does not favor scattering events. And therefore the anisotropic magnetoresistance is dominating. The long Néel wall tail influences the magnetization behavior as this is a source of an intrinsic magnetic field transverse to the long edge of the stripe [32]. The magnetization inside the implanted stripe is tilted towards the magnetization direction inside the nonimplanted stripe as a consequence of the transverse field generated by the Néel domain tail [Fig. 5(c)]. The resistance of the domain wall itself, however, cannot be isolated from the resistance of the magnetic domains with this approach. Finally, the resistance is decreasing with increasing field until the second stripe type switches. The second step of the hysteresis is correlated to the switching of the nonimplanted stripes; see Fig. 5(d). The reversal results in an increase of the AMR [visible shortly after field point (d)]. The inset of Fig. 5 (upper) displays the measurement if the current is applied parallel to the long

edge of the stripes. Again a two-step switching reversal of the magnetization along the stripe axis is observed. In contrast to the measurement before the relative resistance (orange curve) has a dip during the antiparallel state. This prooves that the AMR contribution, due to the magnetization tilt of the domain tail, is dominating the resistance change of the domain wall.

In addition a detailed investigation of the maximum during the two-step reversal process was performed. As mentioned before, the maximum was recorded for samples for which the stripe width of the implanted and nonimplanted stripes was varied from 8 to 22 μm with both stripe types having the same width. In Fig. 6, two-dimensional (2D) color plots of the AMR measurement as a function of field and field angle are shown. The color code visualizes the resistance. A red color depicts a high AMR and blue depicts a low AMR. A typical resistance performance for a permalloy film of the same thickness is given in Fig. 6(a) for reference. At low field values and angles up to 30° (close to the current direction), the resistance has a pronounced minimum during the magnetization reversal. For field angles above 30° the resistance as a function of field becomes almost constant. Figure 6(b) shows the resistance as function of the field angle and magnitude for a sample, where all stripes have the same width of 16 μm. A signature similar to the unstructured reference sample is still visible. But in addition there is an increase of the AMR during magnetization reversal. This AMR maximum, which was described in Fig. 5, is clearly resolved in the plot. The AMR peak occurs between 0 and 0.4 mT field and in the angle range of 5°–60°. Therefore, for every field sweep between 5° and 60°, it was possible to observe the AMR maximum during reversal as described in Fig. 5. Only in the case that the field is applied off axis does separate switching of the different stripe types occur resulting in the observed maximum. Figure 6(c) is discussed in the next subsection.

To analyze this group of peaks the following procedure was applied: (i) The peak height was determined as the normalized difference between the resistance minimum and maximum for all field angles. (ii) From this set the largest peak height was considered as the maximum of the sample. The results for various samples are shown in Fig. 6(c). w denotes the width of the stripe. The x axis $(w_{imp} + w_{nonimp})^{-1}$ corresponds to the domain-wall density, assuming one domain wall between each implanted and nonimplanted stripe. This means the thinner the stripes are, the higher the number of domain walls in the same area is. This implies that a higher density of domain walls results in a higher resistance. Note that in our case the presence of domain walls yields a positive contribution, which could be discussed in the context of the AMR effect of the dominating domain-wall tail.

In contrast to the measurements shown in Fig. 3 where the AMR has a symmetric behavior, the AMR follows now an s-shaped curve (orange curve, Fig. 7). This is due to the fact that for Fig. 3 the sample had stripe widths of 20 μm | 15 μm (implanted | nonimplanted) and for Fig. 7 the stripe widths are 30 μm | 20 μm (implanted | nonimplanted), respectively. Therefore the AMR of Fig. 7 shows an antisymmetric resistance behavior, which has a linear dependence between −0.3 and 0.3 mT. Such a hybrid stripe structure can therefore be used as a sensor.

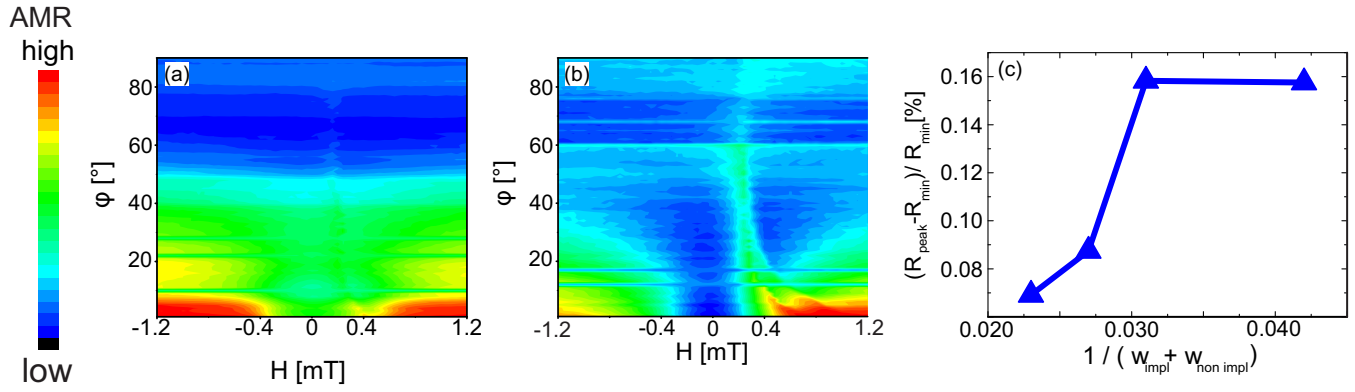Yet, also a magnetization reversal loop of the x component similar to the one shown in Fig. 3 is visible.

FIG. 6. Measurement of the AMR at different field angles φ for (a) a permalloy film and (b) a stripe sample with $w = 16\ \mu$m | 16 μm (implanted | nonimplanted) stripes. (c) Dependence of the height of the extra peak at the interface on the sum of implanted and nonimplanted stripe width ($w_{\mathrm{imp}} + w_{\mathrm{nonimp}}$).

To understand the difference, the magnetic domain images yield important information. In addition to the difference in saturation magnetization between the implanted stripes to the nonimplanted ones the implanted stripes have a reduced film thickness due to partial sputtering of the sample surface of about few nm. This does result in an edge between them. For Figs. 7(a)–7(e) there is a domain parallel to the long edge of the stripe visible. This specific domain type was measured for this sample and other samples where the stripe width of both stripe types is equal and in between 22 and 12 μm. The width of this domain is small when the field is high [Figs. 7(a) and 7(e)] and the largest for zero field [Fig. 7(c)]. This is the typical characteristic of an edge domain. The edge domains consist of Néel-domain walls, under the conditions of an easy axis in the stripe direction, high enough demagnetization fields at the stripe edge, and field applied perpendicular to the stripe length [33]. They can occur at the edge of a stripe because the demagnetization field there is higher compared to the center of the stripe [32].

To understand the input of the domain pattern on the AMR a method to calculate the AMR response from Kerr images was developed.
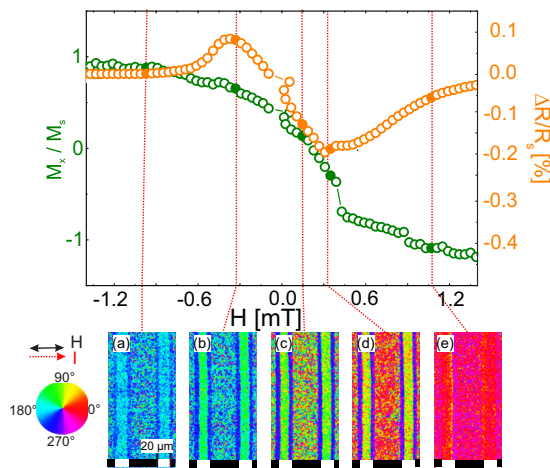
B. Contact-free AMR measurement

Magnetic domain images have been recorded by using separate wavelengths, i.e., red and blue for the x and y plane of incidence, respectively. Under the assumption of in-plane magnetization only it is possible to quantitatively reconstruct the magnetic domain image. From the quantitative domain images the in-plane magnetization angle of every single pixel of the image can be deduced.

For the calculation of the AMR these angles are needed. Every image pixel within the selected region of interest (ROI) is treated as a resistance value. The total resistance of the ROI was calculated by first connecting all pixels (resistors) in parallel to the current direction. And the second step was to apply a series connection of the resulting values to obtain the total resistance of each ROI. This information can be used in order to calculate the AMR for a given current direction. For the calculation it is assumed that the current flows perpendicular to the stripe edge. Figure 8 shows two examples for which the calculated AMR is compared to the measured one. The measurements were performed on stripe structures for which two different stripe orientations were combined on a single substrate (see icons inside Fig. 8). The stripe width was chosen to be 8 μm [Fig. 8(a)] and 2 μm [Fig. 8(b)]. The field was applied in two different directions, parallel to the current [Fig. 8(a)] and perpendicular to the current [Fig. 8(b)]. Both measurements exhibit a good agreement of the directly measured curve (orange) with the calculated one (black).
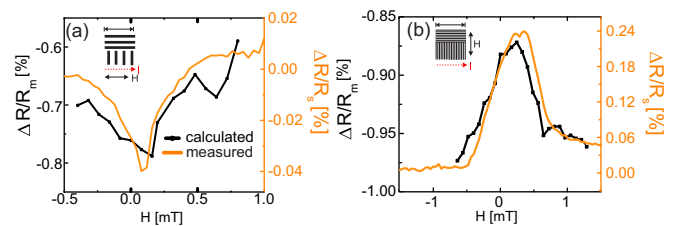

FIG. 7. AMR measurements on sample with $w = 30\ \mu$m | 20 μm (implanted | nonimplanted) stripes and $\varphi_H = 0°$. R_s is the resistance of the sample measured at magnetic saturation in $\varphi_H = 0°$ direction.

FIG. 8. Comparison of directly measured AMR and AMR calculated from Kerr images for composite stripe structures of series 4 with (a) $w = 8\ \mu$m stripes and $\varphi_H = 0°$ and (b) $w = 2\ \mu$m stripes and $\varphi_H = 90°$.
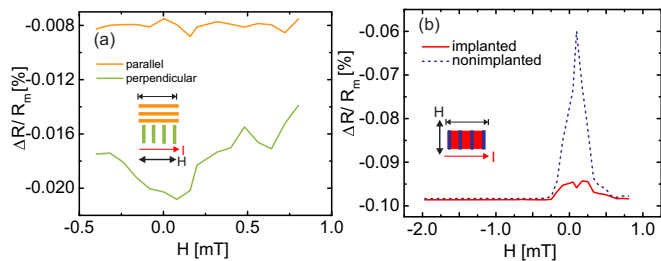
FIG. 9. Comparison of calculated AMR composite stripe structures (series 4). (a) Influence of stripe orientation for $w = 8\,\mu$m and $\varphi_H = 0°$ and (b) influence of implantation for $w = 2\,\mu$m and $\varphi_H = 0°$.

One advantage of this contact-free method is that the individual contributions, i.e., single stripes, of the AMR can now be studied. For the calculation shown in Fig. 9(a) the contribution from stripes oriented parallel to the current (orange curve) and perpendicular to the current (green curve) were separated. The stripes, which are oriented perpendicularly to the field and current, do have a higher impact on the AMR as compared to those being oriented parallel.

With this method it is now also feasible to compare the AMR of an implanted stripe to the AMR of a nonimplanted one [see Fig. 9(b)]. This is achieved simply by selecting a region of interest within a stripe. The dashed line, which shows a higher value during the reversal process, belongs to the nonimplanted stripes. It can be concluded that the AMR is reduced when permalloy is implanted with Cr ions, which is in qualitative agreement with the finding of Nagura *et al.* [34].

IV. SUMMARY

In this work the AMR and microscopic magnetic domain configuration of magnetic hybrid structures were simultaneously investigated. The magnetic patterning was performed by local ion implantation. This modifies the magnetic domain structure and thus influences the response of the resistance.

When the field is applied parallel to the current a separate switching of the implanted stripes with respect to the non-implanted stripes was found. This separate switching leads to a resistance maximum. Further investigations of this additional AMR maximum for different stripe widths supports the assumption of a positive domain-wall resistance behavior. For stripes below 8 μm no extra AMR peak was detected and no separate switching of the implanted and the nonimplanted stripes was observed. The anisotropy of the hybrid structures also influences the AMR response. When the anisotropy axis is parallel to the stripe axis an asymmetric resistance was measured. In another measurement the asymmetric resistance curve was attributed to the occurrence of edge domains.

Furthermore, we developed a method for contact-free AMR measurements of a region of interest. This was realized by quantitative magnetic domain observation with dual-wavelength Kerr microscopy. The AMR was obtained from magnetization angle calculations for each image pixel. It is demonstrated that the nonimplanted stripes give a higher AMR response than the implanted ones. Moreover, the AMR response of stripes oriented perpendicular to the field and current direction was found to be lower than the parallel oriented ones.

We believe that magnetic hybrid structures are good candidates to tune the AMR response by influencing the domain pattern. As demonstrated in this work, this can be done by modifying the magnetic parameters of individual stripes. In this respect, contact-free AMR calculations may act as an efficient tool for the resistance optimization.

[1] M. Bolte, M. Steiner, C. Pels, M. Barthelmess, J. Kruse, U. Merkt, G. Meier, M. Holz, and D. Pfannkuche, Phys. Rev. B **72**, 224436 (2005).

[2] C. Nam, J. Korean Phys. Soc. **63**, 441 (2013).

[3] K. Meng, J. Xiao, Y. Wu, J. Miao, X. Xu, J. Zhao, and Y. Jiang, Sci. Rep. **6**, 20522 (2016).

[4] H.-l. Liu, T. Škereň, A. Volodin, K. Temst, A. Vantomme, and C. Van Haesendonck, Phys. Rev. B **91**, 104403 (2015).

[5] J. Kwon, S. Goolaup, F. Tan, C. Chang, K. Roy, and W. Lew, Curr. Appl. Phys. **17**, 98 (2017).

[6] W. Thomson, Proc. R. Soc. London **8**, 546 (1857).

[7] S. Andreev and P. Dimitrova, J. Optoelectron. Adv. Mater. **7**, 199 (2005).

[8] H. Fujiwara, Y. Sugita, and N. Saito, Appl. Phys. Lett. **4**, 199 (1964).

[9] B. Obry, T. Meyer, P. Pirro, T. Brächer, B. Lägel, J. Osten, T. Strache, J. Fassbender, and B. Hillebrands, Appl. Phys. Lett. **102**, 022409 (2013).

[10] B. Obry, P. Pirro, T. Brächer, A. V. Chumak, J. Osten, F. Ciubotaru, A. A. Serga, J. Fassbender, and B. Hillebrands, Appl. Phys. Lett. **102**, 202403 (2013).

[11] J. McCord, L. Schulze, and J. Fassbender, Adv. Mater. **20**, 2090 (2008).

[12] M. Langer, K. Wagner, T. Sebastian, R. Hübner, J. Grenzer, Y. Wang, T. Kubota, T. Schneider, S. Stienen, K. Lenz, H. Schultheiß, J. Lindner, K. Takanashi, R. E. Arias, and J. Fassbender, Appl. Phys. Lett. **108**, 102402 (2016).

[13] T. Manago, K. Kanazawa, and T. Kera, J. Magn. Magn. Mater. **321**, 2327 (2009).

[14] G. Tatara and H. Fukuyama, Phys. Rev. Lett. **78**, 3773 (1997).

[15] A. K. Patra, A. von Bieren, S. Krzyk, J. Rhensius, L. J. Heyderman, R. Hoffmann, and M. Kläui, Phys. Rev. B **82**, 134447 (2010).

[16] P. M. Levy and S. Zhang, Phys. Rev. Lett. **79**, 5110 (1997).

[17] M. Viret, D. Vignoles, D. Cole, J. M. D. Coey, W. Allen, D. S. Daniel, and J. F. Gregg, Phys. Rev. B **53**, 8464 (1996).

[18] J. Trützschler, K. Sentosun, M. Langer, I. Mönch, R. Mattheis, J. Fassbender, and J. McCord, J. Appl. Phys. **115**, 103901 (2014).

[19] A. Beguivin, H. Corte-Leon, A. Manzin, V. Nabaei, P. Krzysteczko, H. Schumacher, D. Petit, R. Cowburn, and O. Kazakova, J. Appl. Phys. **115**, 17C718 (2014).

[20] M. R. R. Azad, A. Kobs, B. Beyersdorff, P. Staeck, G. Hoffmann, R. Frömter, and H. P. Oepen, Phys. Rev. B **90**, 014404 (2014).

[21] J. Akerman, M. Muñoz, M. Maicas, and J. L. Prieto, J. Appl. Phys. **115**, 183909 (2014).

[22] J. Osten, K. Lenz, A. Henschke, J. Lindner, and J. Fassbender, Rev. Sci. Instrum. **85**, 123701 (2014).

[23] A. K. Majumdar and P. v. Blanckenhagen, Phys. Rev. B **29**, 4079 (1984).

[24] J. Fassbender, J. von Borany, A. Mücklich, K. Potzger, W. Möller, J. McCord, L. Schultz, and R. Mattheis, Phys. Rev. B **73**, 184410 (2006).

[25] N. Martin, I. Mönch, R. Schäfer, J. Fassbender, L. Schultz, and J. McCord, Phys. Rev. B **83**, 174423 (2011).

[26] J. McCord, J. Phys. D: Appl. Phys. **48**, 333001 (2015).

[27] Note that the AMR was measured over the complete sample (0.25 mm^2, while the field of view for the domain images was 0.03 mm^2.

[28] J. Fassbender, T. Strache, M. O. Liedke, D. Marko, S. Wintz, K. Lenz, A. Keller, S. Facsko, I. Mönch, and J. McCord, New J. Phys. **11**, 125002 (2009).

[29] J. Fassbender and J. McCord, J. Magn. Magn. Mater. **320**, 579 (2008).

[30] R. Collette, J. Appl. Phys. **35**, 3294 (1964).

[31] C. Hassel, S. Stienen, F. M. Römer, R. Meckenstock, G. Dumpich, and J. Lindner, Appl. Phys. Lett. **95**, 032504 (2009).

[32] A. Hubert and R. Schäfer, *Magnetic Domains - The Analysis of Magnetic Microstructures* (Springer, Berlin, 2000).

[33] R. Mattheis, K. Ramstäck, and J. McCord, IEEE Trans. Magn. **33**, 3993 (1997).

[34] H. Nagura, K. Saito, K. Takanashi, and H. Fujimori, J. Magn. Magn. Mater. **212**, 53 (2000).